NASA TECHNICAL NOTE

NASA TN D-4713

c1

NASA TN D-4713

TECH LIBRARY KAFB, NM

0131286

LOAN COPY: RETURN TO
AFWL (WLIL-2)
KIRTLAND AFB, N MEX

FLIGHT-TEST ANALYSIS OF APOLLO HEAT-SHIELD MATERIAL USING THE PACEMAKER VEHICLE SYSTEM

by Randolph A. Graves, Jr., and William G. Witte

Langley Research Center
Langley Station, Hampton, Va.

NATIONAL AERONAUTICS AND SPACE ADMINISTRATION • WASHINGTON, D. C. • AUGUST 1968

TECH LIBRARY KAFB, NM

0131286

NASA TN D-4713

FLIGHT-TEST ANALYSIS OF APOLLO HEAT-SHIELD MATERIAL USING THE PACEMAKER VEHICLE SYSTEM

By Randolph A. Graves, Jr., and William G. Witte

Langley Research Center
Langley Station, Hampton, Va.

NATIONAL AERONAUTICS AND SPACE ADMINISTRATION

For sale by the Clearinghouse for Federal Scientific and Technical Information
Springfield, Virginia 22151 – CFSTI price $3.00

FLIGHT-TEST ANALYSIS OF APOLLO HEAT-SHIELD MATERIAL USING THE PACEMAKER VEHICLE SYSTEM

By Randolph A. Graves, Jr., and William G. Witte
Langley Research Center

SUMMARY

The Apollo heat-shield material was flight tested on the hemispherically blunted nose cap of a Pacemaker vehicle. Ablation and temperature data were obtained at the stagnation point and at the 22.5°, 45°, and 67.5° stations. Maximum pressures at these locations were 8.4, 6.7, 4.1, and 1.7, atmospheres, respectively. (1 atm = 101 325 N/m^2.) Recession rates at the 22.5°, 45°, and 67.5° stations were greater than predicted, and this result is attributed to the high levels of turbulent aerodynamic shear, which exceeded the threshold shear sensitivity of this material. Unequal absorption of the surface sealer into the porous heat-shield material modified its behavior and introduced uncertainties in the analysis during the early portions of the data period.

INTRODUCTION

Langley Research Center is engaged in a long-range study of heat-shield materials for the purpose of developing materials for specific applications and also to develop analytical models that will adequately predict ablation performance. The Pacemaker project is a research program within this long-range study. The environment produced by the present Pacemaker launch vehicle is such that flight levels of heating rate, enthalpy, and pressure are within the ranges attainable in existing ground facilities. This feature narrows the gap between ground-test environment and flight environment, and thereby makes possible an early evaluation of predictions of ablator performance based on tests in ground facilities.

At present, there is a great interest in developing low-density heat-shield materials for spacecraft reentry. These materials have been shown to provide good thermal-protection systems. A low-density material of particular interest at present is the Apollo heat-shield material, Avcoat 5026-39/HC-G. A series of tests in ground facilities indicated that the performance of this material deteriorates at pressures above atmospheric levels. The R-4 flight-test results in reference 1 seemed to confirm this relationship between rapid erosion and high pressures. The present paper reports the results of a

flight test of the material on the nose cap of a Pacemaker vehicle and reexamines the pressure-erosion relationship in the light of new evidence concerning the effects of shear.

SYMBOLS

A	frequency factor, 1/sec
C_f	skin-friction coefficient
E	activation energy, Btu/mol (joules/mole)
F_C	weight fraction of free carbon in char
G	constant in diffusion-limited oxidation equation
H	heat-transfer coefficient, lbm/ft^2-sec (kilograms/meter^2-second)
h	enthalpy, Btu/lbm (joules/kilogram)
K_O	oxygen mass fraction
M_C	molecular weight of carbon
M_O	molecular weight of oxygen
$\dot{m}$	mass-loss rate, lbm/ft^2-sec (kilograms/meter^2-second)
N	order of reaction
N_{Pr}	Prandtl number
N_{Re}	Reynolds number
p	pressure, lbf/ft^2 (newtons/meter^2)
q	heating rate, Btu/ft^2-sec (watts/meter^2)
R	universal gas constant, Btu/mol-$^{\circ}$R (joules/mole-$^{\circ}$K)

R_{eff}	effective nose radius, ft (meters)
$\dot{s}$	recession rate of ablator surface, ft/sec (meters/second)
T	absolute temperature, ^{o}R (^{o}K)
U	velocity, ft/sec (meters/second)
V	volume, ft^3 ($meters^3$)
W	weight, lbm (kilograms)
η_r	recovery factor
μ	viscosity, lbm/ft-sec (newtons second/$meter^2$)
ρ	density, lbm/ft^3 ($kilograms/meter^3$)
τ	aerodynamic shear, lbf/ft^2 ($newtons/meter^2$)
ψ	convective blocking function

Subscripts:

c	combustion
cw	cold wall
DL	diffusion limited
e	local (edge of boundary layer)
H_2O	water
RL	rate limited
s	stagnation
se	sealer

t	total
vp	porous ablator
vp,se	porous ablator with absorbed sealer
w	wall

Superscript:

*	reference condition

MODEL AND INSTRUMENTATION

The model (fig. 1) was a hemispherically blunted 10° cone with a cylindrical afterbody. The entire model was covered with Avcoat 5026-39/HC-G. However, only the nose cap was instrumented. Figure 2 shows the locations of the ablation sensors and thermocouples in the nose cap. Reference 2 gives a detailed description of the design and fabrication of the model.

A nine-channel telemeter was housed in the section aft of the model. The telemeter transmitted four channels of acceleration data, four channels of ablation data, and one channel of temperature data. The four acceleration-data channels provided continuous data from four accelerometers. Two accelerometers provided thrust and drag measurements, while two others provided measurements of the transverse accelerations.

The four ablation-data channels and the one temperature-data channel were commutated at a rate of approximately six times per second. This permitted a total of 48 ablation measurements plus commutated data from 11 thermocouples. The 48 ablation measurements were made with 32 make-wire sensors arranged in four eight-element assemblies, eight light-pipe sensors in two four-element assemblies, and eight spring-wire sensors in two four-element assemblies. A complete description of the ablation sensors and their operation can be found in reference 3. The thermocouples were chromel-alumel and were of the same design as those in reference 4. In addition to the nose-cap thermocouples, one other thermocouple was located internally on the bulkhead as shown in figure 1.

LAUNCH VEHICLE AND OPERATIONS

The propulsion system of the Pacemaker launch vehicle consists of four stages of solid-propellant rocket motors: Honest John, Nike, TX-77, and Recruit. Reference 5

contains a description of the system. A photograph of the Pacemaker vehicle and model in launch position is shown in figure 3. The vehicle was launched October 15, 1965, from the NASA Wallops Island launch facility. It was launched at an elevation angle of 77° on an azimuth of 110°. A plot of the flight trajectory is shown in figure 4. The sequence of trajectory events is also indicated in figure 4 and shown in greater detail in table I.

The variations of flight velocity and altitude as determined from radar tracking data are shown in figure 5. Two C-band beacons on the payload facilitated tracking. A rawinsonde launched prior to flight measured ambient pressure and temperature. These measured values were within 3 percent of corresponding values in the U.S. Standard Atmosphere (ref. 6).

HEATING ANALYSIS

The resultant angle of attack of the model during reentry was computed from the normal and transverse accelerations, the reentry trajectory, and the model configuration and aerodynamic characteristics. These computations indicate that the model was flying in an angle-of-attack envelope of $\pm 3^{\circ}$. Since this angle-of-attack envelope is relatively small, the local flow and heating conditions are based on a zero angle of attack.

The heating rates at the off-stagnation locations were calculated for turbulent flow because previously recovered Pacemaker flight models (ref. 5) have surface recessions that indicate turbulent flow conditions for the flights. Reference 7 presents results of ground tests which also indicate that transitional and turbulent flow are probable at these flight conditions.

The heating rates for locations away from the stagnation point are calculated by Eckert's reference-enthalpy method as outlined in reference 8, where

$$h^* = 0.5h_e + 0.5h_w + 0.22\eta_r \frac{U_e^2}{2} \tag{1}$$

and $\eta_r = 0.892$ for turbulent flow. This local enthalpy and local pressure are used to determine all other reference thermodynamic properties. The local heat-transfer coefficients as functions of a skin-friction factor are calculated by using Reynolds' analogy and a Stanton number based on the enthalpy difference, as in reference 9, so that

$$H = \frac{C_f \rho U}{2N_{Pr}^{2/3}} \tag{2}$$

The turbulent incompressible skin-friction factor is given by the Schultz-Grunow relationship, as in reference 10, as

$$C_f = \frac{0.370}{\left(\log_{10} N_{Re}\right)^{2.584}} \tag{3}$$

In Eckert's reference-enthalpy method (ref. 8), the effects of compressibility can be accounted for by introducing the property values at the reference condition. Thus the turbulent heat-transfer coefficient is

$$H = \frac{0.185\rho^* U_e}{N_{Pr}^{2/3}\left(\log_{10} N_{Re}^*\right)^{2.584}} \tag{4}$$

The calculated turbulent heating rates are for flat plates with locally constant pressure and temperature. Nevertheless, these expressions can be used in regions of strong pressure and temperature gradients. This is demonstrated in reference 11, which shows good correlation between calculations made by this method and flight-test results for axisymmetric blunt bodies. Turbulent aerodynamic shears were obtained by use of

$$\tau_w = \frac{C_f \rho^* \left(U_e\right)^2}{2} \tag{5}$$

where the incompressible skin-friction coefficient is obtained from flow properties at reference conditions, as in reference 8.

The stagnation heating calculations were based on the initial hemispherical nose radius and the transport properties of reference 12. The method used to calculate the heating is that of reference 13, presented here in the nomenclature of the present paper:

$$H = \frac{0.767\left(\rho_s \mu_s\right)^{0.43}\left(\rho_w \mu_w\right)^{0.07}}{R_{eff}^{0.5} N_{Pr}^{0.6}}\left(\frac{2p_s}{\rho_s}\right)^{0.25} \tag{6}$$

where

$$\frac{q_w}{h_T - h_w} = H \tag{7}$$

and the cold-wall heating is defined as

$$q_{cw} = Hh_t \tag{8}$$

The laminar heating rates for the 22.5°, 45°, and 67.5° stations were computed manually by using the ratios of local to stagnation heat-transfer rate presented in reference 14.

The results of the heat-transfer calculations are presented in figure 6 for the stagnation point and for the local stations with both laminar and turbulent flow. The local Reynolds number based on wetted distance from the stagnation point is presented in figure 7 for the 22.5°, 45°, and 67.5° stations, while the turbulent shear computations for these stations are presented in figure 8.

It should be noted that the computations presented here are for a hemispherical nose cap. However, during the flight, surface recession was unequal across the nose cap. Therefore, these computations are applicable with certainty only until some time less than halfway through the data period.

ABLATION ANALYSIS

The ablation predictions were made with the aid of a computer program derived from the one described in reference 15. The program treats ablation as a one-dimensional transient heat-conduction problem with internal decomposition. The surface recession can be specified in several manners, but for this analysis only surface recession due to char oxidation was considered. Briefly, the equations governing the char-layer oxidation are:

In the rate-controlled regime,

$$\dot{m}_{c,RL} = \frac{A}{F_C} p_e^{N_c} K_{O,e}^{N_c} \exp\left(\frac{\Delta E}{RT_w}\right) \tag{9}$$

where the rate constants used for the oxidation of Avcoat 5026-39/HC-G are

$$A = 1.74 \times 10^5 \text{ per second}$$

$$N_c = \frac{1}{2}$$

$$\frac{\Delta E}{R} = 32\ 800^\circ \text{ R} \quad (18\ 222^\circ \text{ K})$$

and

$$F_C = \frac{\rho(\text{carbon in char})}{\rho(\text{char})}$$

In the diffusion-controlled regime,

$$\dot{m}_{c,DL} = GK_{O,e}\psi H \tag{10}$$

where

$$G = \frac{M_C}{M_O}\frac{1}{F_C}$$

The total char loss is obtained from

$$\left(\frac{1}{\dot{m}_c}\right)^{1/N_c} = \left(\frac{1}{\dot{m}_{c,RL}}\right)^{1/N_c} + \left(\frac{1}{\dot{m}_{c,DL}}\right)^{1/N_c} \tag{11}$$

The surface recession is obtained from the total char mass-loss rate by

$$\dot{s} = \frac{\dot{m}_c}{\rho_{(char)}} \tag{12}$$

MATERIAL DESCRIPTION

Avcoat 5026-39/HC-G is an epoxy novolac resin with special additives in a fiberglass honeycomb matrix. In fabrication, the empty honeycomb is bonded to the primary structure and the resin is gunned into each cell individually. Reference 2 contains a description of the material fabrication. The overall density of the material is 32 lb/ft^3 (512 kg/m^3).

The char of the material is composed mainly of silica and carbon. It is necessary to know the amounts of each in the char because in the ablation analysis the silica is considered to be inert, but the carbon is considered to enter into exothermic reactions with oxygen. The char was obtained by a thermogravimetric analysis. The results are shown in figure 9, where the percentage of weight remaining is plotted as a function of temperature for a heat rise of the material of 39.6° R (22° K) per minute. At 2160° R (1200° K), 54 percent by weight of the virgin material has volatilized and 46 percent has remained as char.

Since the calculated surface temperatures exceeded 2160° R (1200° K) during the flight, a 46-percent char yield was used to determine a char density of 14.7 lb/ft^3 (238 kg/m^3). In the virgin material, 25 percent by weight is silica, and since the silica is considered to be inert the char-layer composition becomes 6.7 lb/ft^3 (107.4 kg/m^3) of carbon and 8 lb/ft^3 (128.1 kg/m^3) of silica.

During the reduction of the flight data it became apparent that the ablator performed much better in the early portions of the data period than had been predicted by either laminar or turbulent theory. In an attempt to explain this behavior, several samples of the virgin material were cored from the flight backup model, which had been fabricated in the same manner as the flight model. Microscopic examination of the cores revealed that surface sealer had penetrated into the porous ablator. Penetration depths varied from 0.0 in some locations to 0.1 inch (2.54 mm) in other locations. The nature of the sealer and the method of application were examined and it was ascertained that some of the inherent properties of the sealer, as well as the method of application, would not lead to either uniform penetration of the sealer or to consistent penetration in the flight and backup models. These inconsistencies made it impossible to specify a definite depth of penetration of the sealer into the ablator on the flight model.

The density changes of the material and char due to the absorption of sealer were analyzed. (See appendix.) The density of the virgin material with absorbed sealer was

47.2 lb/ft^3 (756.0 kg/m^3). The carbon char yield for this resin system was approximately 27.5 percent so that the carbon density in the char was 10.75 lb/ft^3 (172.2 kg/m^3). These values were used in the initial data portions of the ablation analysis.

RESULTS AND DISCUSSION

The ablation and thermocouple results (event times) obtained during the flight are presented in tables II and III. All the ablation sensors were activated. Figure 10 shows the plotted results for the stagnation point and for the 22.5°, 45°, and 67.5° stations. The spring-wire and light-pipe sensors measure surface recession. The make-wire sensors normally measure char interface recession. But, as pointed out in reference 3, in severe environments where a thick char is unable to form, make-wire sensors for all practical purposes measure surface recession. Ground tests indicate that at the high shear levels and heating rates of the present test a mature char does not form on Avcoat 5026-39/HC-G. Therefore, all the sensors were interpreted as measuring surface recession.

During the data period, it is conjectured, the heat-shield material was removed so rapidly that a sharp temperature gradient existed near the surface of the material. Therefore, the thermocouples embedded in the material showed no responses until the surface receded to their locations. Then their responses, as indicated on the thermocouple traces, were either a deflection beyond the full-scale calibration signal, or hash indicating a broken junction. As a result, no temperature histories in the material were obtained. Rather, the instant when the trace indicated that the thermocouple measured surface or boundary-layer temperatures or went out of order was taken to be the time when the surface receded past the hot junction of the thermocouple. These data are given in table III and are also plotted in figure 10.

The Avcoat 5026-39/HC-G, as will be developed in the following paragraphs, showed four ablation regimes:

(1) A reduced rate of ablation due to the enhancement of the physical properties of the material by absorption of the surface sealer

(2) What might be called an abnormally high rate of ablation at the stagnation point as compared with present calculations

(3) An "accelerated" rate of ablation at the 22.5°, 45°, and 67.5° stations

(4) A "catastrophic" rate of ablation at the 45° and 67.5° stations, for unknown reasons

In figure 11 the ablation data for the three locations have been replotted along with oxidation-theory recession predictions computed with and without the effects of the absorption of the surface sealer into the heat-shield material. Presented also in figure 11(a) is

the stagnation-point recession based on a correlation of high-pressure ground tests. This correlation shows slightly less recession than the corresponding oxidation theory.

In figures 11(b) and (c) the replotted ablation data for the 45° and 67.5° stations are shown along with oxidation-theory predictions based on laminar heating and based on turbulent heating with and without sealer effects. The surface recession predicted for laminar heating was much less than the recession that actually occurred and also less than that predicted for turbulent heating. Even poorer agreement would have been realized if sealer effects had been used with laminar heating. Thus the turbulent-heating assumption made earlier gives surface recessions that are more in line with the flight data. When the sealer effects are included in the turbulent-heating assumption, correlation is obtained with the initial portions of the data.

In figure 12 the flight data are compared with the most reasonable recession predictions for the three locations. In figure 11 curves were faired through all the data for the stagnation point and through the main body of data points for the 45° and 67.5° stations. The intersections of these curves with the prediction curves calculated by oxidation theory including sealer effects were assumed to be the points in time at which the sealer no longer affected the ablation results. Since the penetration of sealer was not necessarily uniform radially at these stations, these points in time are average values. The predictions of surface recession past these points were calculated with the original material densities. These predictions (shown in fig. 12) are in poor agreement with the flight data.

If the remaining thicknesses of material at given times are taken from the curves faired through the data in figure 12, a sequence of surface outlines can be constructed as shown in figure 13. Ablation was assumed to be uniform radially at the stations of concern, so that the nose cap remained symmetrical about its axis of revolution. The dashed lines connecting the data points are based on the sequential changes of similar configurations tested in ground facilities.

As shown in figure 13, considerably less ablation occurs at the stagnation point than at the other stations on the nose cap. This results in a smaller effective nose radius at the stagnation point and an increased stagnation-point heating rate. By the time of 87.0 seconds, the computed stagnation-point heating rate shown in figure 6 is lower than the actual rate. This discrepancy partially explains why the predicted recession distance at the stagnation point was less than the measured distance. However, a satisfactory means of correcting the stagnation-point heating was not ascertained.

In figures 12(b) and (c) it can be seen that the surface recessions during the period of "accelerated" ablation vary consistently from the greatest recession at the 22.5° station to the least recession at the 67.5° station. The recession rates also vary consistently, being 0.235 in./sec (0.597 cm/sec), 0.224 in./sec (0.567 cm/sec), and

0.203 in./sec (0.516 cm/sec), at the 22.5°, 45°, and 67.5° stations, respectively, during this period. In figure 6 it is seen that the surface recessions also vary consistently with heating rate, but heating rate alone is not sufficient to cause the very large recessions. Unpublished ground-test results indicate that this material becomes shear sensitive at a shear level of approximately 15 lb/ft^2 (718.2 N/m^2). The computed turbulent shear levels for these stations exceed this threshold sensitivity during the period of "accelerated" ablation. (See fig. 8.) The authors hypothesize that once the shear-sensitivity level is exceeded the ablator no longer has the protection of a mature char layer; that is, the surface is sheared off at or in the pyrolysis zone. Thus the recession rates would be largely determined by the pyrolysis rate of the virgin material. Since the pyrolysis rate is determined by the rate of heat input, the recession rate of the virgin material in the absence of a char layer is a function of local heating. The consistent variation of recession with heating rate tends to support this hypothesis.

The surface recessions for the off-stagnation locations also vary consistently with local pressure (see fig. 14), but this result is believed to be only coincidental. If pressure had been the important mechanism, the stagnation point would have had the largest recession since it had the greatest pressure level.

The final portions of the faired curves for the 45° and 67.5° stations indicate a catastrophic failure of the material. In both cases the curves end when the remaining thickness is 0.65 inch (1.65 cm). These final points on the curves correspond to the locations of the innermost thermocouples in the material at these stations. The curves could be extended to zero if it were known that the heat-shield material was removed completely at these times. It is likely that this happened. At 95.5 seconds, the thermocouple on the bulkhead inside the model exceeded the range for which it was calibrated. (See fig. 15.) This was probably due to hot gases entering the model interior through a hole burned through the inconel skin of the nose cap. However, the failure of the heat-shield material cannot be related to the changing environmental conditions that were computed for a hemispherical nose shape.

CONCLUDING REMARKS

Avcoat 5026-39/HC-G was flight tested on the nose cap of a Pacemaker vehicle with temperature and ablation measurements obtained at four locations. From the present analysis it appears that the surface recessions at the three off-stagnation stations are due to a combination of aerodynamic shear and heating rate. Although many uncertainties are present in the analysis, the removal of the char layer by aerodynamic shear was believed to be the controlling mechanism for surface recession.

Apparently, a catastrophic failure of the heat-shield material occurred during the latter portion of the data period. However, this failure cannot be related to the changing environmental conditions that were computed for the hemispherical nose shape.

Unequal absorption of the surface sealer into the porous heat-shield material modified its behavior and introduced uncertainties in the analysis during the early portions of the data period.

Langley Research Center,
National Aeronautics and Space Administration,
Langley Station, Hampton, Va., May 21, 1968,
709-09-00-01-23.

APPENDIX

SURFACE-SEALER EFFECTS

The surface sealer applied to the porous ablator to prevent moisture absorption itself penetrated the ablator. The resin system of the sealer is identical with that of the ablator so that the effect of this sealer was to increase the virgin-material density and char yield. In order to determine the effects of the sealer it was necessary to know the amount of sealer that could be absorbed by the ablator. From liquid-water absorption tests it was determined that the weight of the ablator increased by a factor of 1.4 when saturated. On the assumption that the resin is absorbed in the same way as water, the following approximate analysis is presented.

The total weight is

$$W_t = W_{vp} + W_{H_2O} \tag{A1}$$

Dividing by total volume gives

$$\frac{W_t}{V_t} = \frac{W_{vp}}{V_t} + \frac{W_{H_2O}}{V_t} \tag{A2}$$

The weight of absorbed water is

$$W_{H_2O} = \rho_{H_2O} V_{H_2O} \tag{A3}$$

so that the total density is

$$\rho_t = \rho_{vp} + \rho_{H_2O} \frac{V_{H_2O}}{V_t} \tag{A4}$$

Since

$$\rho_t = 1.4\rho_{vp} \qquad \rho_{H_2O} \approx 2\rho_{vp}$$

it follows that

$$1.4\rho_{vp} = \rho_{vp} + 2\rho_{vp} \frac{V_{H_2O}}{V_t} \tag{A5}$$

and the fractional volume of water is

$$\frac{V_{H_2O}}{V_t} = 0.2 \tag{A6}$$

The density of the porous ablator with absorbed sealer is

$$\rho_{vp,se} = \rho_{vp} + \frac{V_{H_2O}}{V_t} \rho_{se} \tag{A7}$$

APPENDIX

The density of the porous ablator is 32 lb/ft^3 (512 kg/m^3), and if the sealer is assumed to be all resin, its density is approximately 76 lb/ft^3 (1217.5 kg/m^3). Therefore the density of the new virgin material is

$$\rho_{cp,se} = 47.2 \text{ lb/ft}^3 \quad (756.1 \text{ kg/m}^3)$$

REFERENCES

1. Brooks, William A., Jr.; Tompkins, Stephen S.; and Swann, Robert T.: Flight and Ground Tests of Apollo Heat-Shield Material. Conference on Langley Research Related to Apollo Mission, NASA SP-101, 1965, pp. 29-44.
2. Guidi, M. A.: Final Summary Fabrication Report on Pacemaker Vehicle. RAD-SR-65-56 (Contract NAS-1-3958), AVCO Corp., Mar. 16, 1965.
3. LeBel, Peter J.; and Russell, James M., III: Development of Sensors to Obtain In-Flight Ablation Measurements of Thermal-Protection Materials. NASA TN D-3686, 1966.
4. Raper, James L.: Results of a Flight Test of the Apollo Heat-Shield Material at 28,000 Feet Per Second. NASA TM X-1182, 1966.
5. Lawrence, George F.; Whitlock, Charles H.; and Walton, Thomas E., Jr.: Aerothermal Measurements of Damaged Reentry Bodies Obtained in Free Flight at Mach Numbers From 11.0 to 2.0. NASA TM X-966, 1964.
6. Anon.: U.S. Standard Atmosphere, 1962. NASA, U.S. Air Force, and U.S. Weather Bur., Dec. 1962.
7. Dunavant, James C.; and Stone, Howard W.: Effect of Roughness on Heat Transfer to Hemisphere Cylinders at Mach Numbers 10.4 and 11.4. NASA TN D-3871, 1967.
8. Eckert, E. R. G.: Engineering Relations for Heat Transfer and Friction in High-Velocity Laminar and Turbulent Boundary-Layer Flow Over Surfaces With Constant Pressure and Temperature. Trans. ASME, vol. 78, no. 6, Aug. 1956, pp. 1273-1283.
9. Colburn, Allan P.: A Method of Correlating Forced Convection Heat Transfer Data and a Comparison With Fluid Friction. Trans. Am. Inst. Chem. Engrs., vol. XXIX, 1933, pp. 174-211.
10. Schlichting, Hermann (J. Kestin, trans.): Boundary Layer Theory. Fourth ed., McGraw-Hill Book Co., Inc., c.1960.
11. Zoby, Ernest V.; and Sullivan, Edward M.: Correlation of Free-Flight Turbulent Heat-Transfer Data From Axisymmetric Bodies With Compressible Flat-Plate Relationships. NASA TN D-3802, 1967.
12. Hansen, C. Frederick.: Approximations for the Thermodynamic and Transport Properties of High-Temperature Air. NASA TR R-50, 1959. (Supersedes NACA TN 4150.)
13. Cohen, Nathaniel B.: Boundary-Layer Similar Solutions and Correlation Equations for Laminar Heat-Transfer Distribution in Equilibrium Air at Velocities up to 41,100 Feet Per Second. NASA TR R-118, 1961.

14. Lees, Lester: Laminar Heat Transfer Over Blunt-Nosed Bodies at Hypersonic Flight Speeds. Jet Propulsion, vol. 26, no. 4, Apr. 1956, pp. 259-269, 274.

15. Wells, P. B.: A Method for Predicting the Thermal Response of Charring Ablation Materials. Doc. No. D2-23256, Boeing Co., 1964.

TABLE I.- SEQUENCE OF TRAJECTORY EVENTS

Event	Time from launch, sec	Altitude		Relative velocity	
		ft	m	ft/sec	m/sec
First-stage ignition	0.0	0	0	0	0
First-stage burnout and drag separation	5.0	4 076	1 242	1 654	504
Second-stage ignition	15.1	16 928	5 160	1 074	327
Second-stage burnout	18.9	22 913	6 984	2 311	704
Apogee	74.8	76 045	23 178	625	190
Third-stage ignition	76.8	75 978	23 158	640	195
Third-stage burnout, fourth-stage ignition, and blast separation of third stage	83.2	72 198	22 005	5 742	1 750
Fourth-stage burnout	85.1	67 525	20 581	10 299	3 139
Model impact	330.0	0	0	60 to 32	18 to 10

TABLE II.- SENSOR DATA

Sensor	Sensor element	Time, sec	Initial depth of sensor	
			in.	cm
Stagnation point				
Light-pipe 1	1	86.87	0.100	0.254
	2	88.12	.205	.521
	3	88.90	.304	.772
	4	90.62	.451	1.146
45° station				
Make-wire 7	1	86.98	0.450	1.143
	2	87.45	.500	1.270
	3	87.62	.550	1.397
	4	87.79	.600	1.524
	5	87.95	.650	1.651
	6	87.96	.700	1.778
	7	87.97	.750	1.905
	8	87.98	.800	2.032
Make-wire 8	1	84.90	0.050	0.127
	2	85.68	.100	.254
	3	86.00	.150	.381
	4	85.86	.200	.508
	5	86.20	.250	.635
	6	86.67	.300	.762
	7	86.84	.350	.889
	8	87.00	.400	1.016
Make-wire 10	1	84.28	0.025	0.064
	2	85.11	.075	.191
	3	85.73	.125	.318
	4	86.05	.175	.444
	5	86.06	.225	.571
	6	86.38	.275	.698
	7	86.54	.325	.825
	8	86.55	.375	.952
Make-wire 11	1	86.72	0.450	1.143
	2	87.35	.500	1.271
	3	87.82	.550	1.397
	4	87.83	.600	1.524
	5	88.02	.650	1.652
	6	88.03	.700	1.779
	7	88.04	.750	1.905
	8	87.90	.800	2.033
67.5° station				
Light-pipe 13	1	86.59	0.145	0.368
	2	87.99	.296	.752
	3	88.31	.452	1.148
	4	88.48	.604	1.535
Spring-wire 15	1	86.86	0.172	0.437
	2	87.19	.321	.815
	3	88.08	.421	1.069
	4	88.99	.624	1.586
Spring-wire 19	1	85.91	0.072	0.182
	2	86.40	.122	.310
	3	86.74	.221	.561
	4	88.57	.521	1.328

TABLE III.- THERMOCOUPLE DATA

Thermocouple number	Time thermocouple goes out, sec	Initial depth of thermocouple	
		in.	cm
22.5° station			
2	87.34	0.600	1.52
3	87.53	.650	1.65
5	88.58	.899	2.28
45° station			
6	87.90	0.749	1.91
9	88.09	.850	2.16
67.5° station			
12	89.48	0.653	1.65
14	88.63	.602	1.52
16	88.30	.650	1.65
17	89.00	.696	1.78
18	88.84	.850	2.16

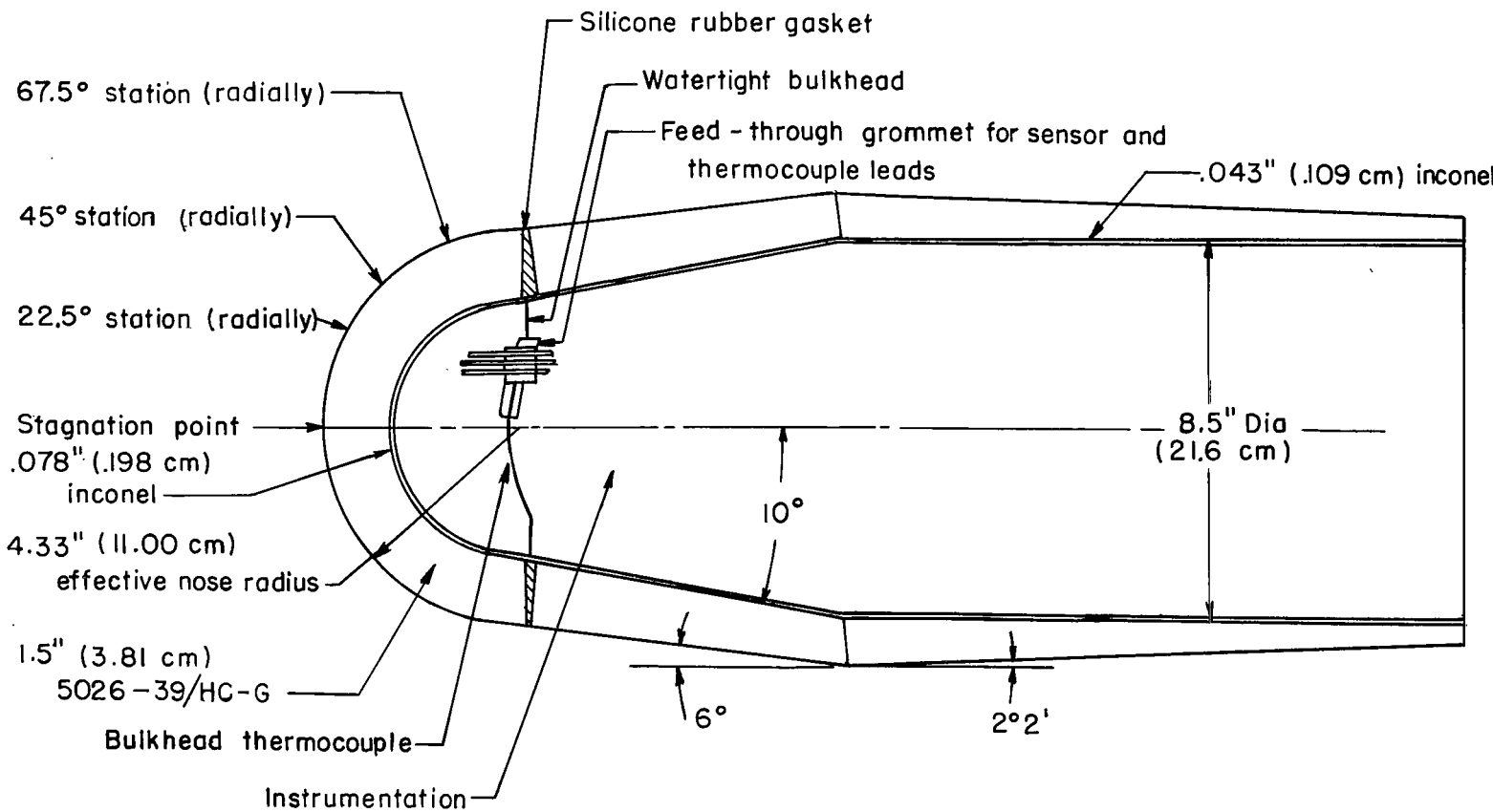

Figure 1.- Sketch of model.

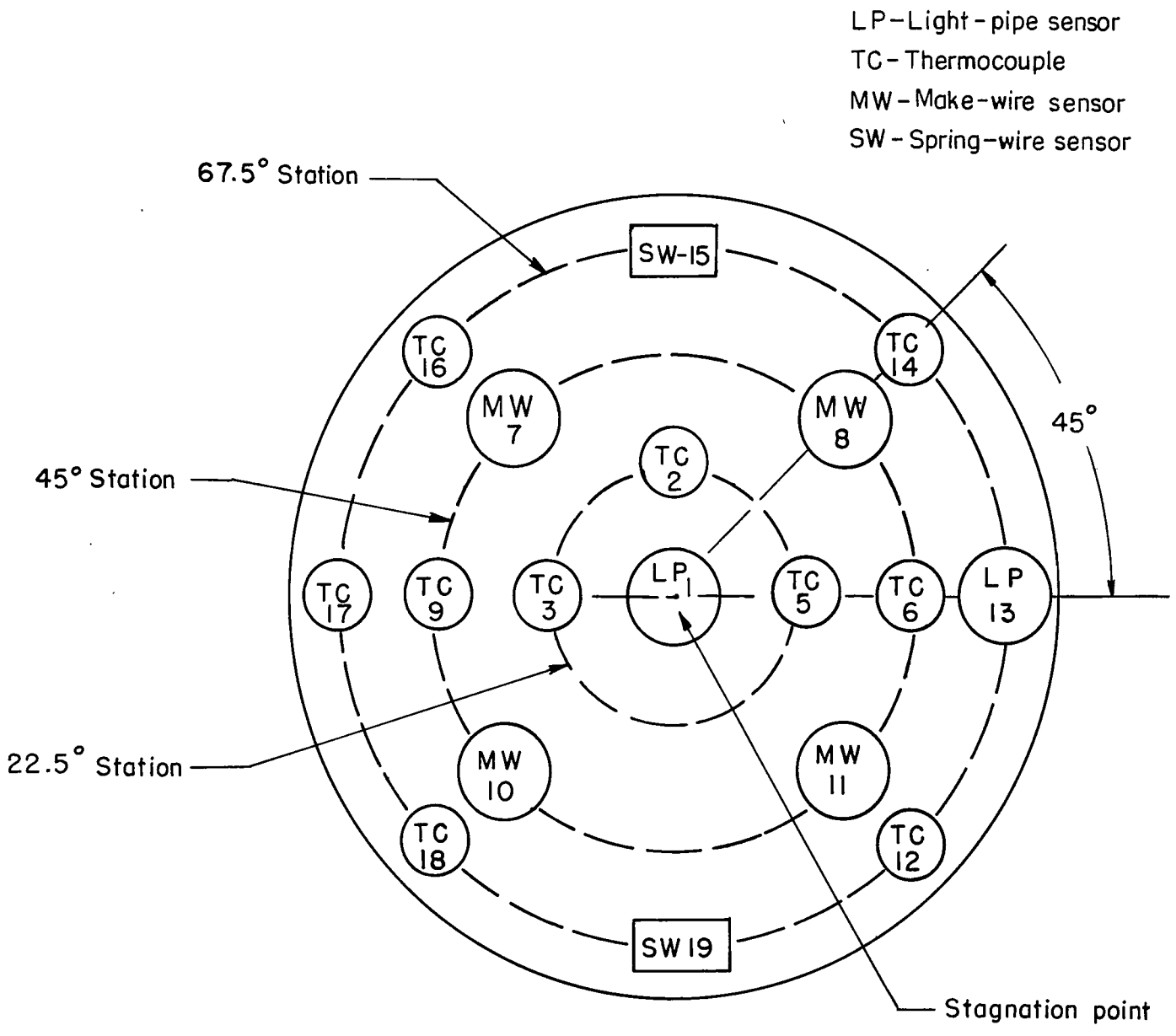

Figure 2.- Sensor and thermocouple locations, viewed from front of model.

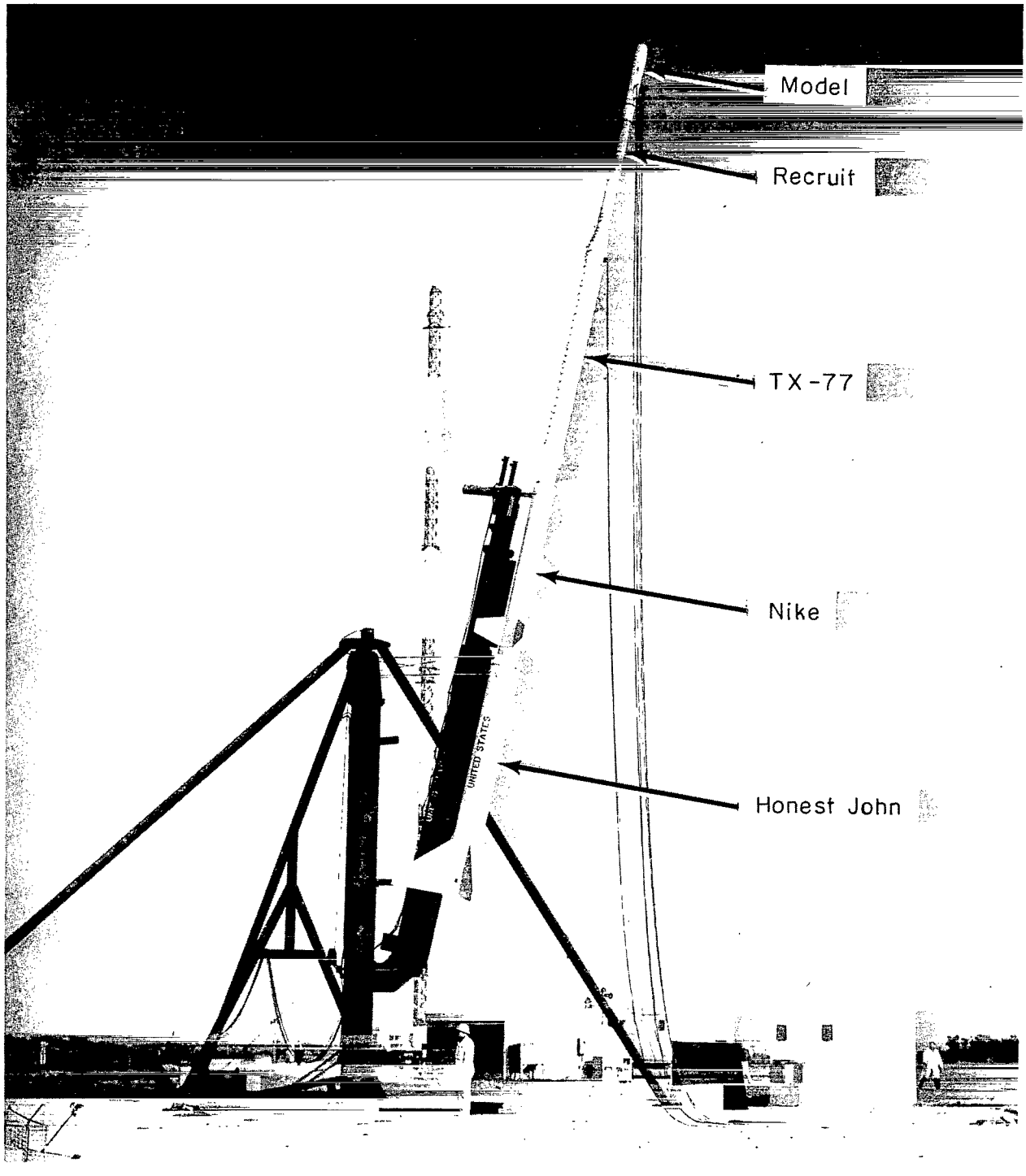

Figure 3.- Pacemaker and model in launch position.

L-65-8080.1

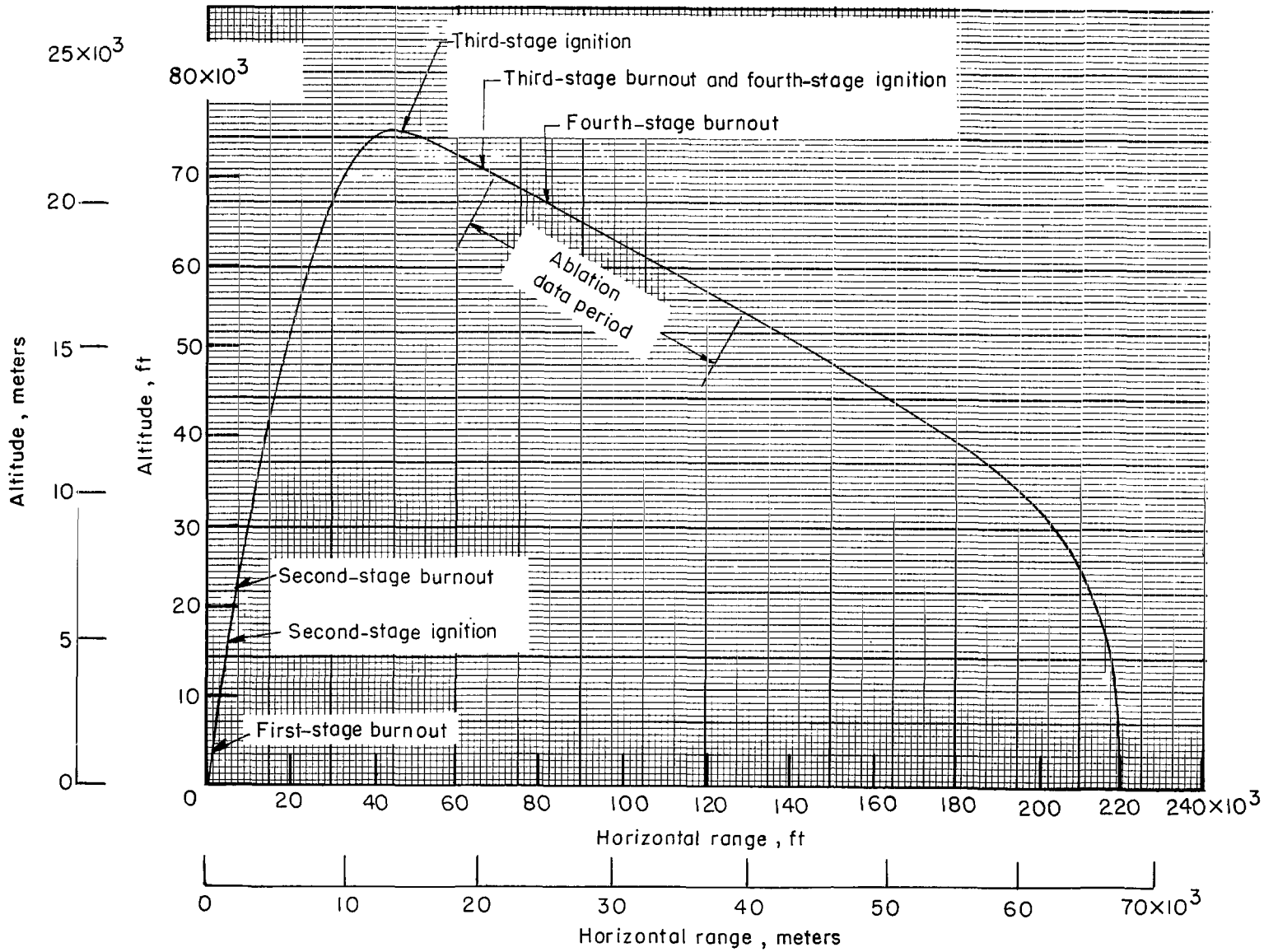

Figure 4.- Flight trajectory.

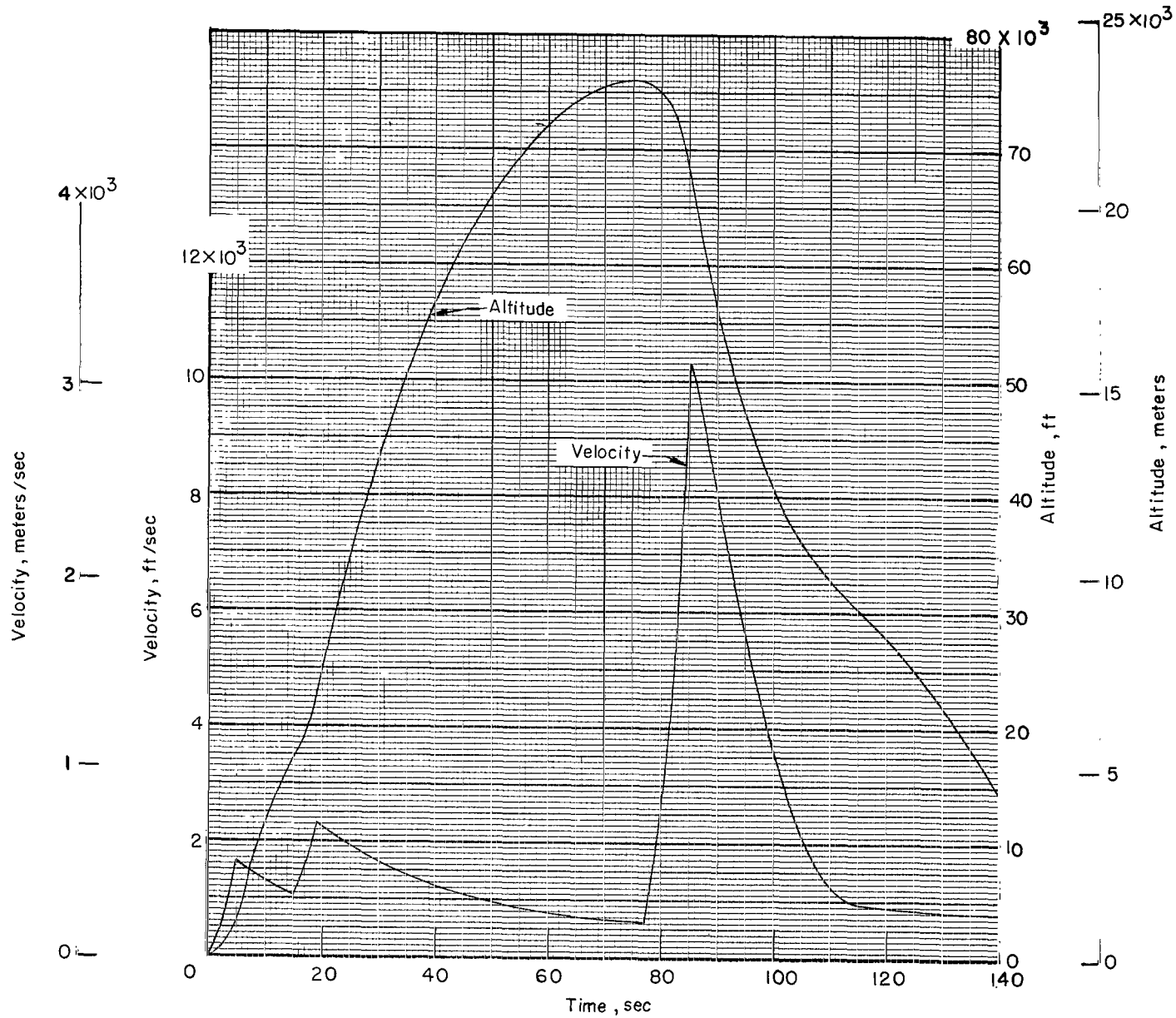

Figure 5.- Time histories of altitude and velocity.

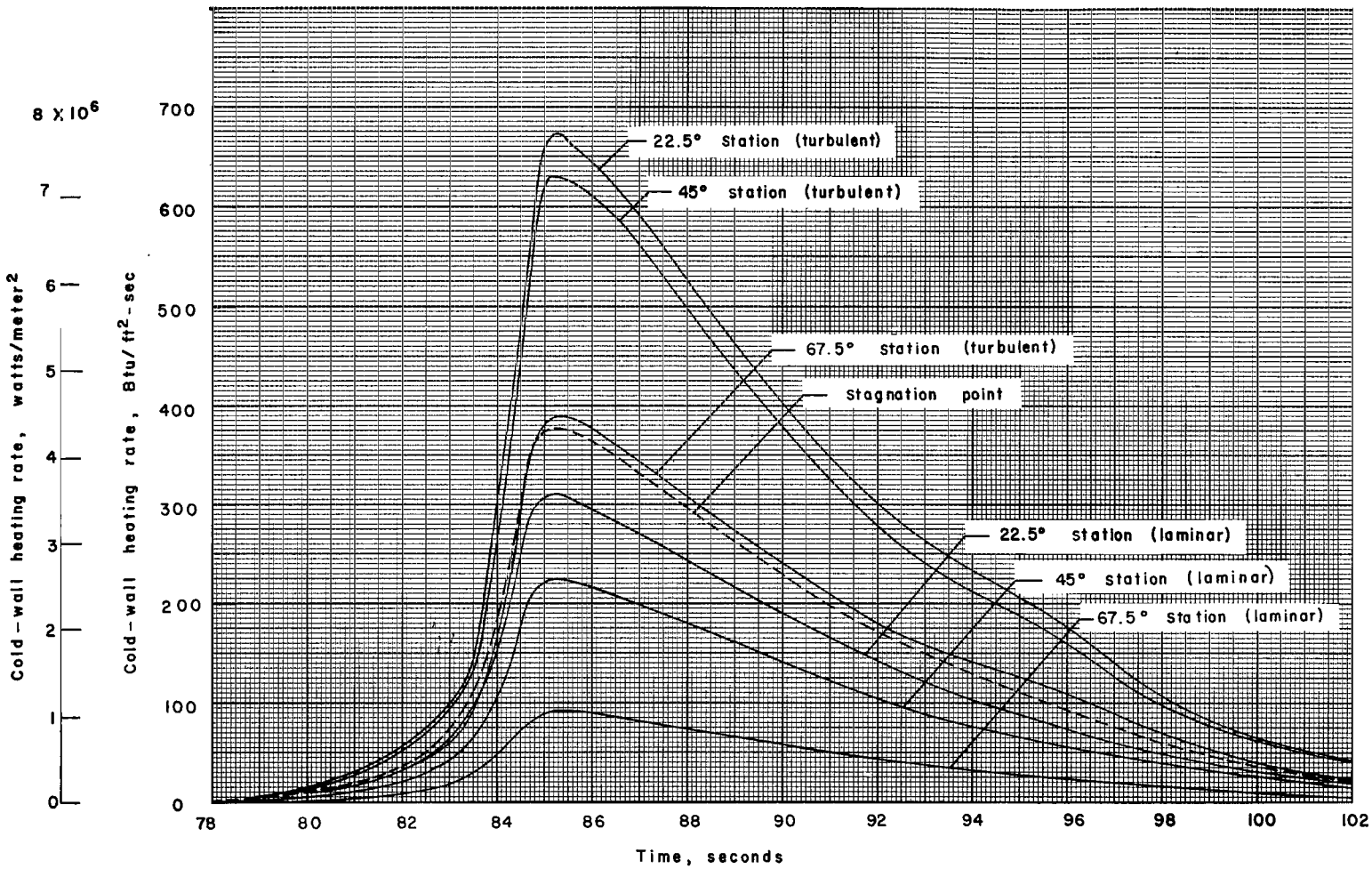

Figure 6.- Computed cold-wall heating rates.

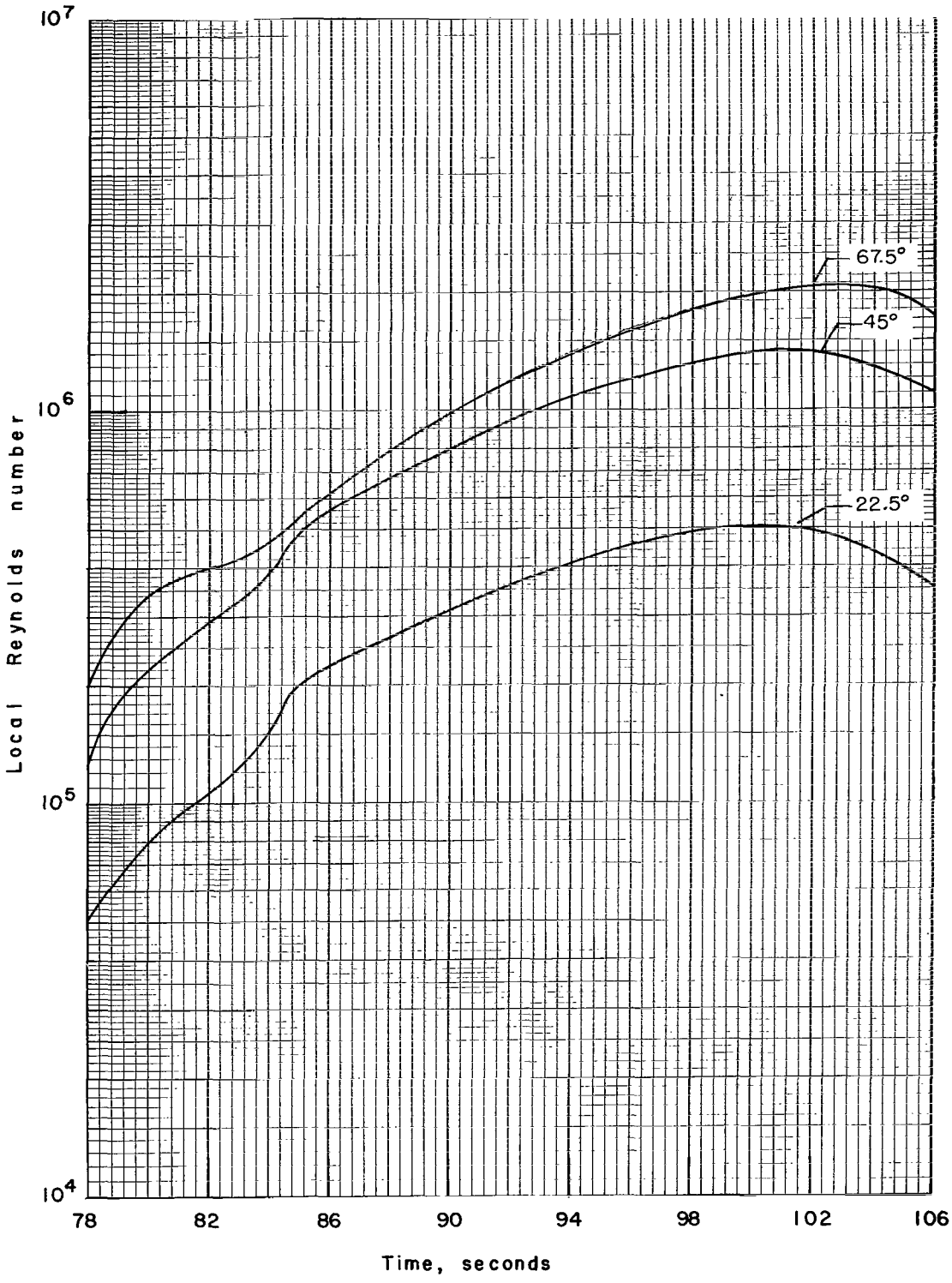

Figure 7.- Computed local Reynolds numbers for stations on the hemispherical nose.

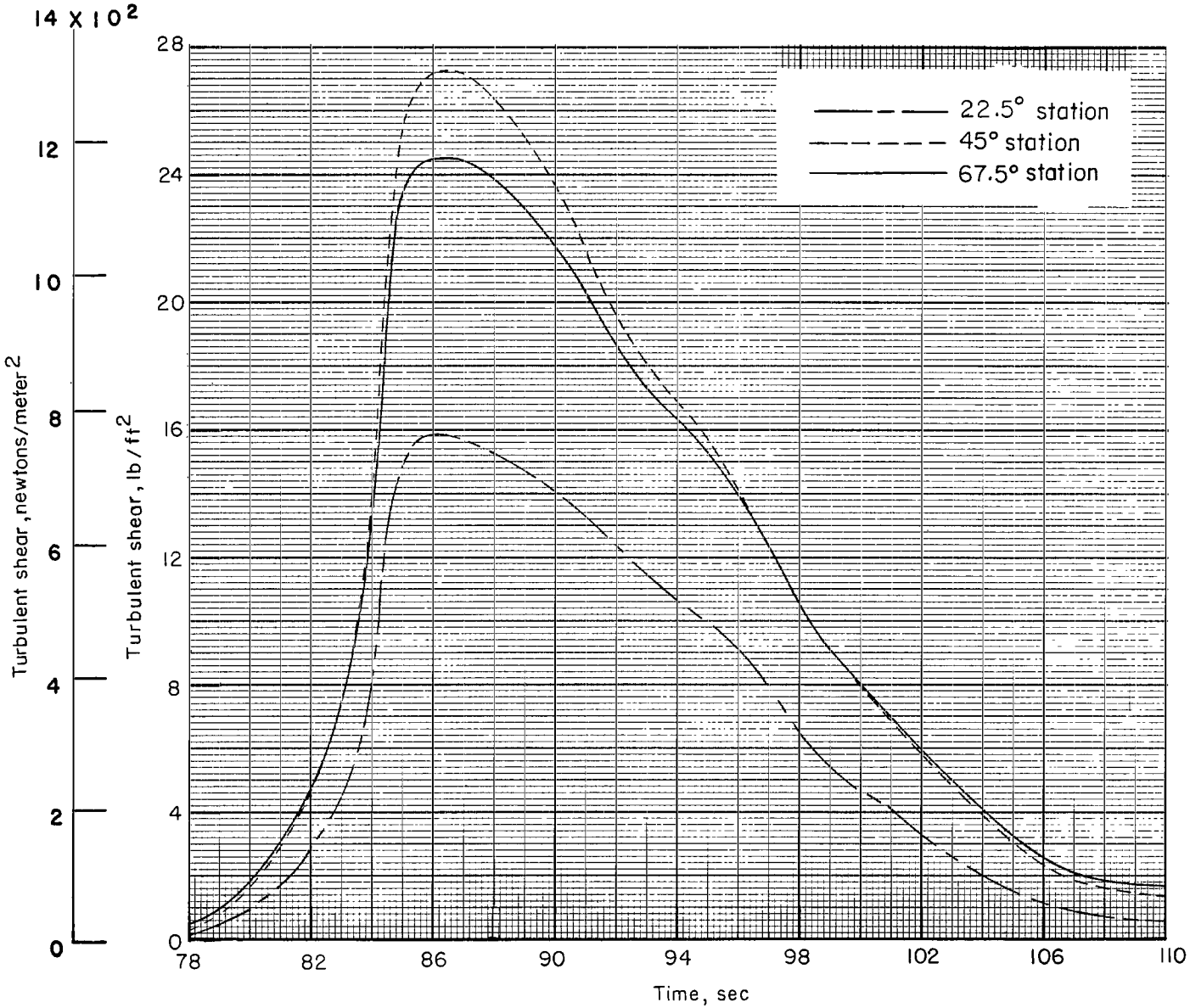

Figure 8.- Computed turbulent aerodynamic shears for stations on the hemispherical nose.

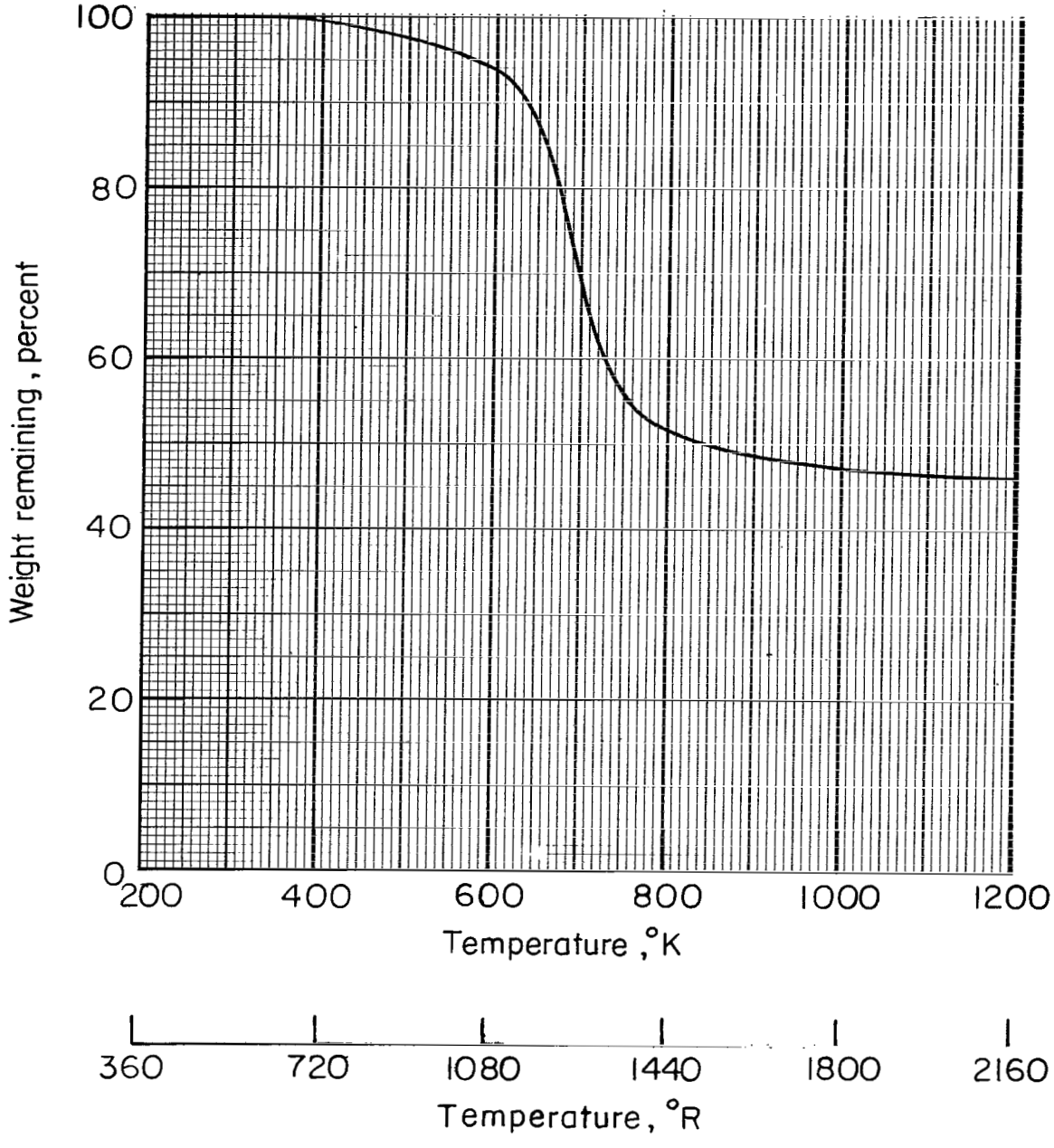

Figure 9.- Percentage of char yield (silica plus carbon) obtained from thermogravimetric analysis. Oven temperature rise, 22° K per minute; helium atmosphere.

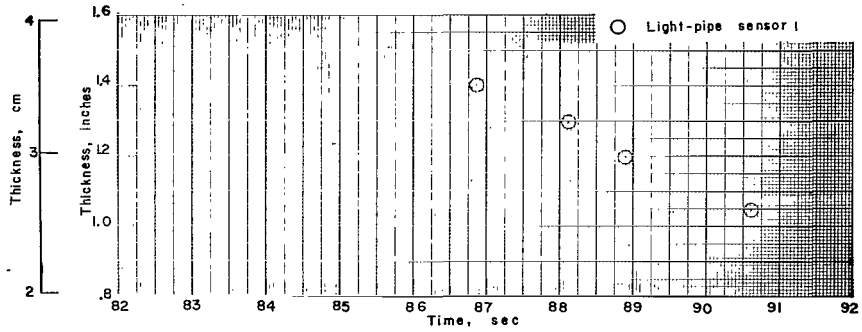

(a) Stagnation point.

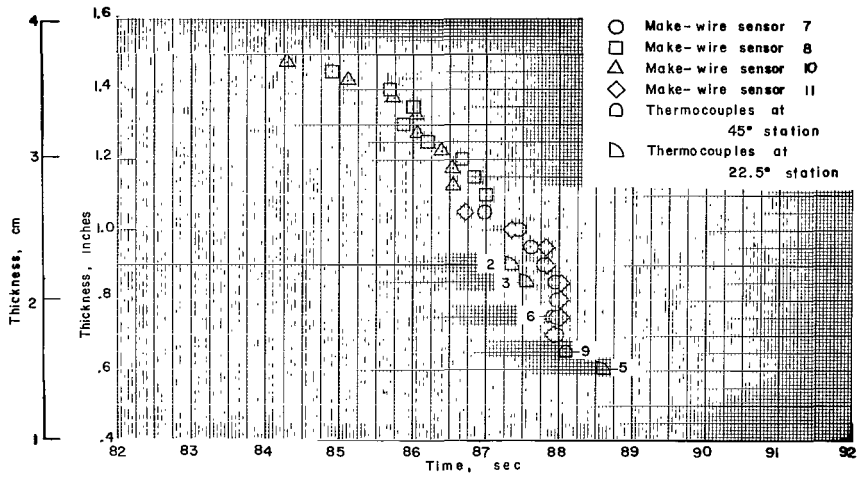

(b) 45^0 station and 22.5^0 station.

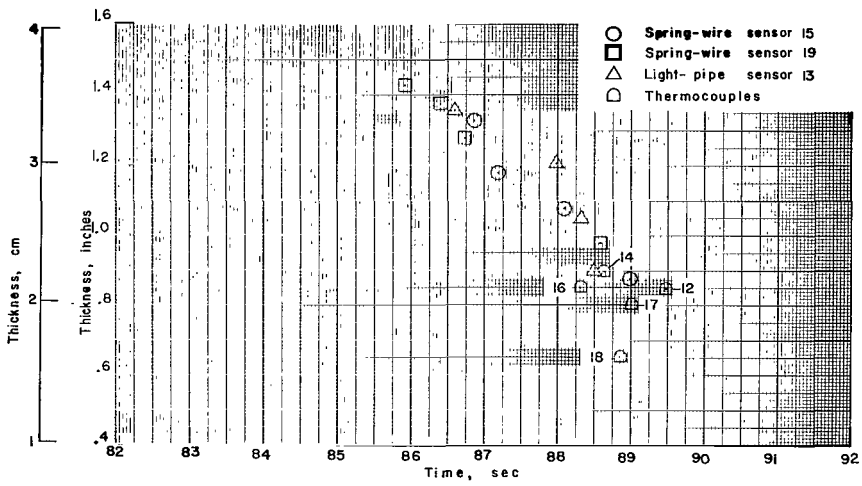

(c) 67.5^0 station.

Figure 10.- Ablation data.

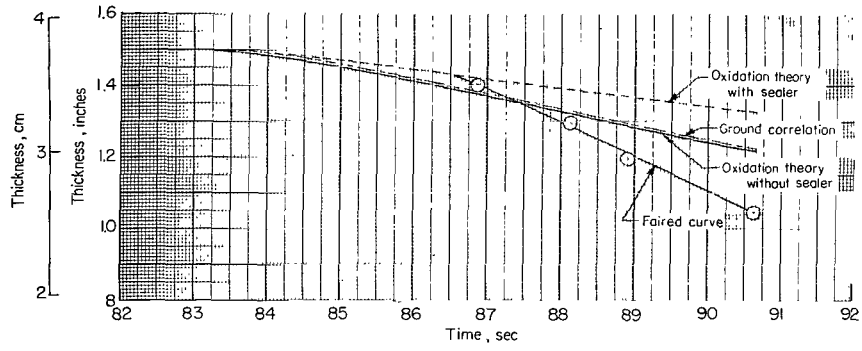

(a) Stagnation point.

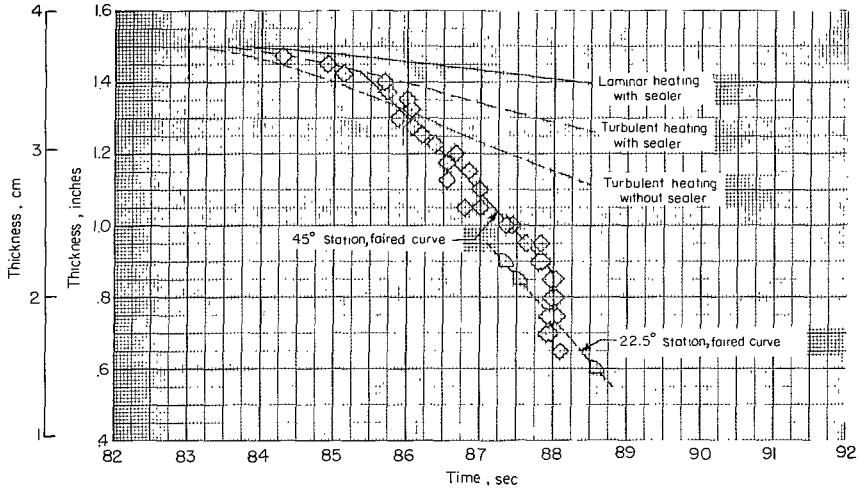

(b) 45° station and 22.5° station; calculations are for 45° station.

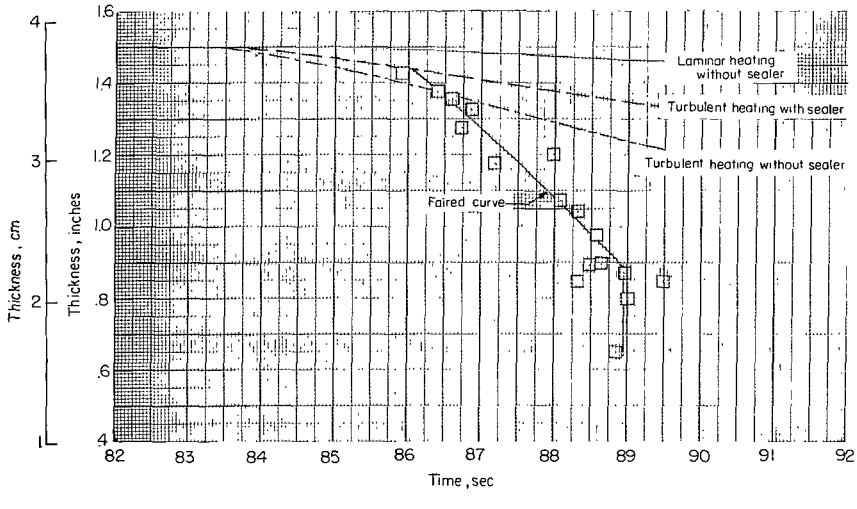

(c) 67.5° station.

Figure 11.- Ablation data, oxidation-theory predictions, and stagnation-point ground correlation.

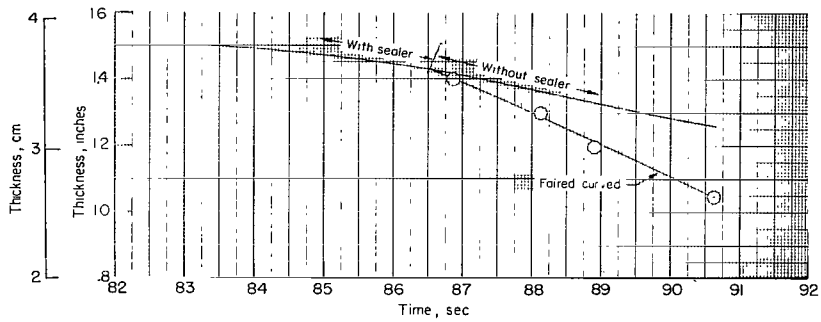

(a) Stagnation point.

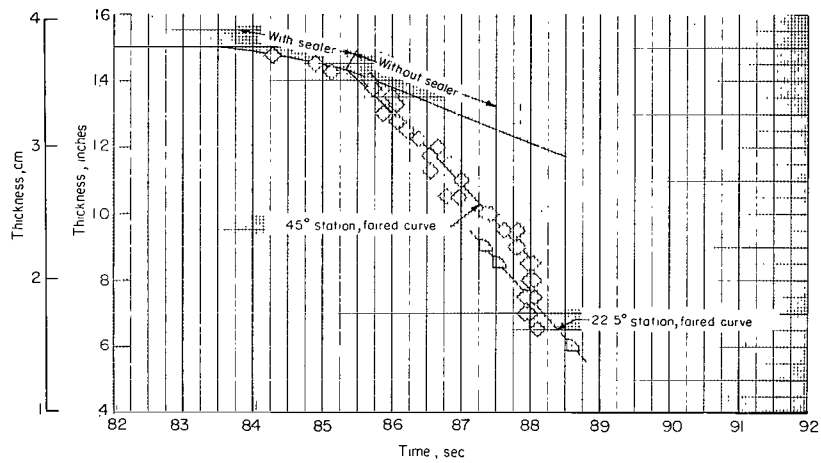

(b) 45° station and 22.5° station; calculations are for 45° station.

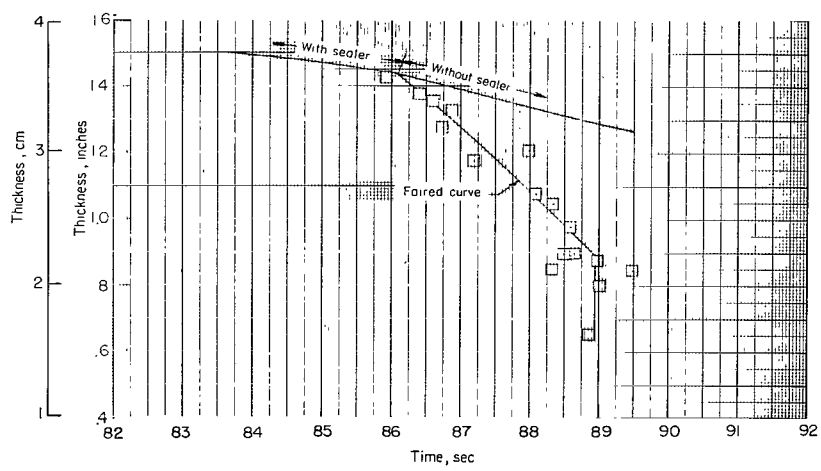

(c) 67.5° station.

Figure 12.- Comparison of the flight data with the most reasonable recession predictions.

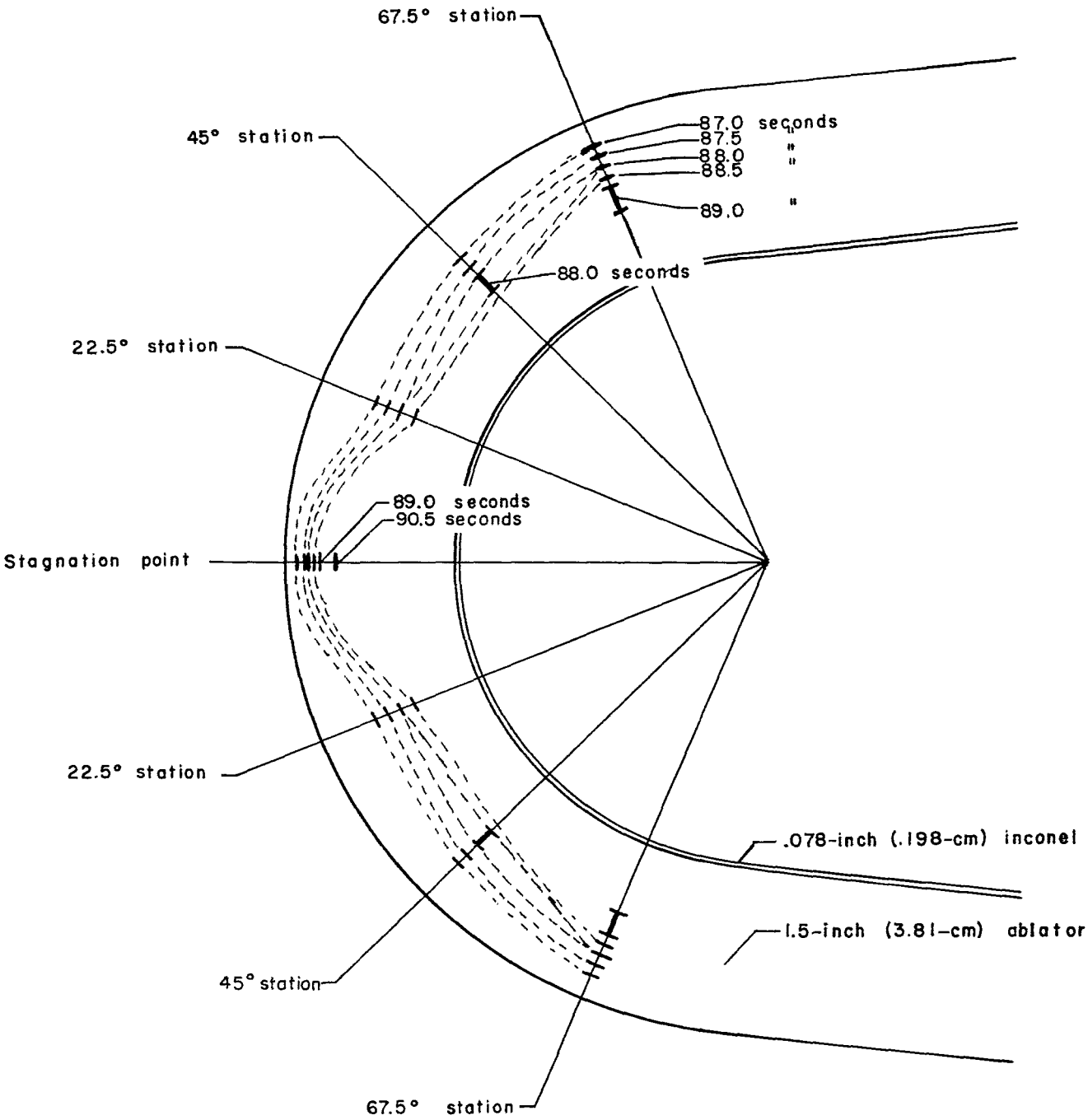

Figure 13.- Sequential changes in surface outlines of the nose cap.

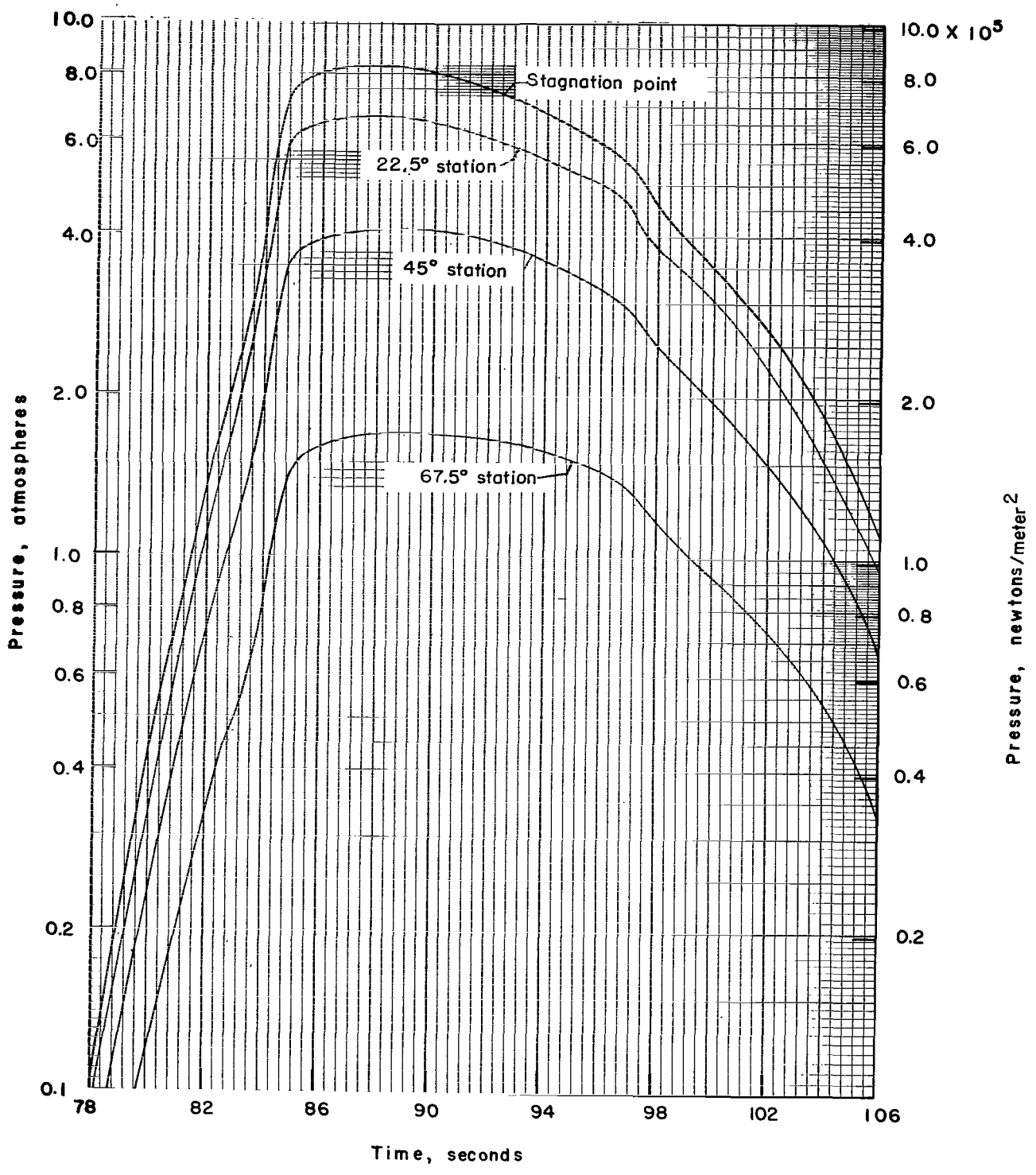

Figure 14.- Computed pressures for stations on the hemispherical nose.

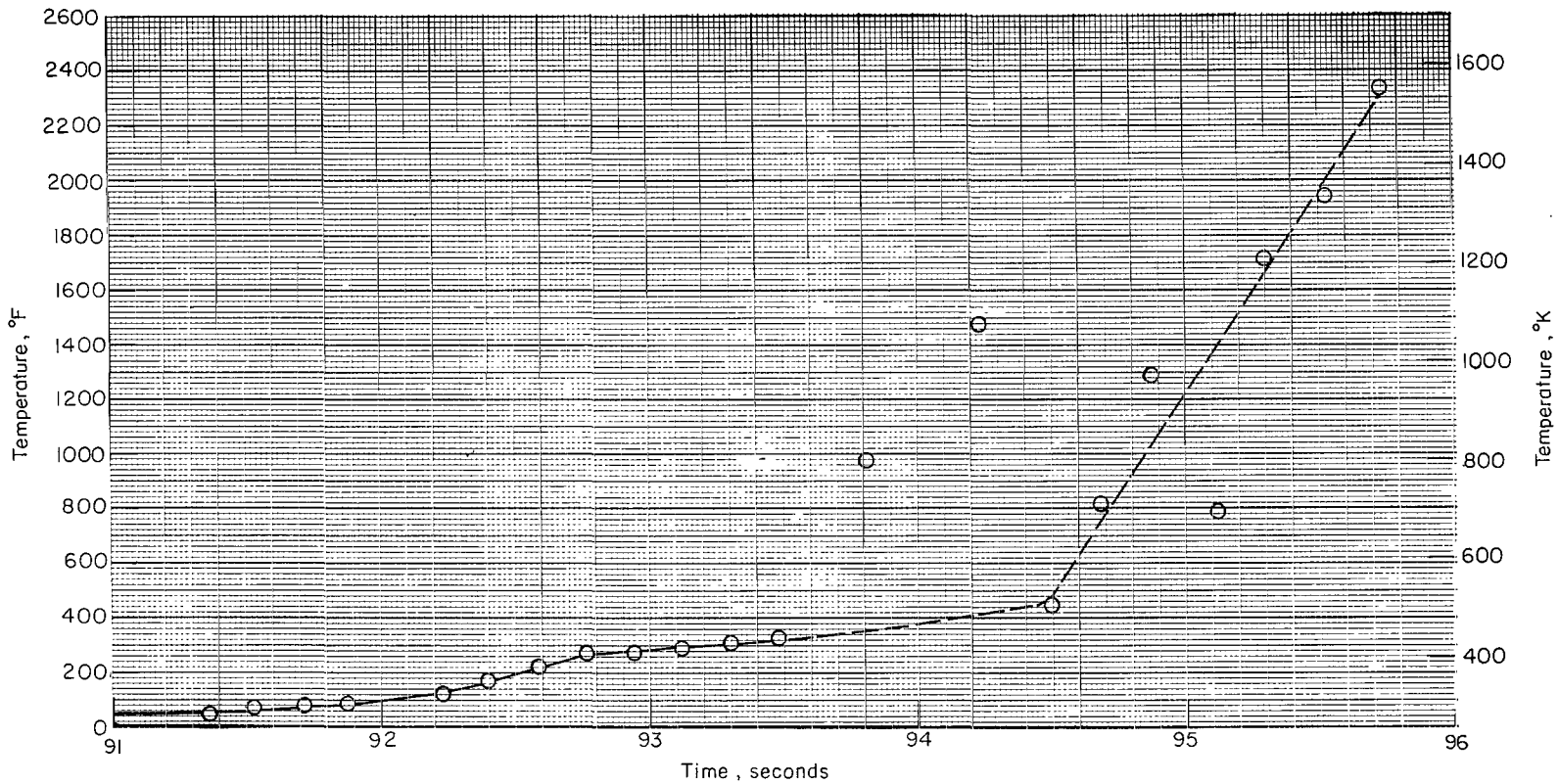

Figure 15.- Bulkhead temperature history.

NATIONAL AERONAUTICS AND SPACE ADMINISTRATION
WASHINGTON, D. C. 20546

OFFICIAL BUSINESS

FIRST CLASS MAIL

POSTAGE AND FEES PAID
NATIONAL AERONAUTICS AND
SPACE ADMINISTRATION

02U 001 58 51 3DS 68194 00903
AIR FORCE WEAPONS LABORATORY/AFWL/
KIRTLAND AIR FORCE BASE, NEW MEXICO 8711.

ATT MISS MADELINE F. CANOVA, CHIEF TECHNI
LIBRARY /WLIL/

POSTMASTER: If Undeliverable (Section 158 Postal Manual) Do Not Return

"The aeronautical and space activities of the United States shall be conducted so as to contribute . . . to the expansion of human knowledge of phenomena in the atmosphere and space. The Administration shall provide for the widest practicable and appropriate dissemination of information concerning its activities and the results thereof."

—NATIONAL AERONAUTICS AND SPACE ACT OF 1958

NASA SCIENTIFIC AND TECHNICAL PUBLICATIONS

TECHNICAL REPORTS: Scientific and technical information considered important, complete, and a lasting contribution to existing knowledge.

TECHNICAL NOTES: Information less broad in scope but nevertheless of importance as a contribution to existing knowledge.

TECHNICAL MEMORANDUMS: Information receiving limited distribution because of preliminary data, security classification, or other reasons.

CONTRACTOR REPORTS: Scientific and technical information generated under a NASA contract or grant and considered an important contribution to existing knowledge.

TECHNICAL TRANSLATIONS: Information published in a foreign language considered to merit NASA distribution in English.

SPECIAL PUBLICATIONS: Information derived from or of value to NASA activities. Publications include conference proceedings, monographs, data compilations, handbooks, sourcebooks, and special bibliographies.

TECHNOLOGY UTILIZATION PUBLICATIONS: Information on technology used by NASA that may be of particular interest in commercial and other non-aerospace applications. Publications include Tech Briefs, Technology Utilization Reports and Notes, and Technology Surveys.

Details on the availability of these publications may be obtained from:

SCIENTIFIC AND TECHNICAL INFORMATION DIVISION

NATIONAL AERONAUTICS AND SPACE ADMINISTRATION

Washington, D.C. 20546